muscles

MDPI

Article

A Simple Model to Predict Loads within Muscle-Tendon Complexes of the Shoulder during Fast Motions

Falk Mörl [1,*,†] and Ingo Bradl [2,†]

[1] Forschungsgesellschaft für Angewandte Systemsicherheit und Arbeitsmedizin mbH, Biomechanik & Ergonomie, Lucas-Cranach-Platz 2, D-99096 Erfurt, Germany
[2] Berufsgenossenschaft Nahrungsmittel und Gastgewerbe, Praevention, Lucas-Cranach-Platz 2, D-99096 Erfurt, Germany; ingo.bradl@fsa.de
* Correspondence: falk.moerl@fsa.de
† These authors contributed equally to this work.

Abstract: The load scenario within the shoulder joint among its muscle–tendon complexes during fast motions is of interest, as it would allow an evaluation of critical, accident-like motions. To enhance knowledge, a modelling approach was carried out and compared to experimental data. Nine subjects were investigated while performing tasks that ranged from easy to demanding. Motions were (1) an easy lift of a small weight, (2) a push against a force measurement device, and (3) a gentle side fall against the immovable force measurement device. Extracted data were the kinematics of the right arm and the contact force on the elbow. A simple direct dynamics shoulder model actuated by Hill-type muscle models was arranged to simulate the three experimental motions. The Hatze-based activation of the muscle models was used without any further simulation of neural regulation. For fast motions, the simple shoulder model predicts well the shoulder angle or contact force values, and data fit well into the variability of the data measured experimentally. Because there was no implementation of more complex neural regulation, slow motions, as performed by the subjects, were, in part, not predicted by the shoulder model. Simple mechanisms can be described by the simple model: When activated, the larger deltoid muscle is able to protect the smaller supraspinatus muscle. Furthermore, in awkward conditions, the gentle side fall against an immovable device alone has enough momentum to damage small muscles.

Keywords: shoulder joint; tendon force; accident like motion; rotator cuff; muscles inner force; behavioural prevention

check for updates

Citation: Mörl, F.; Bradl, I. A Simple Model to Predict Loads within Muscle-Tendon Complexes of the Shoulder during Fast Motions. *Muscles* **2022**, *1*, 50–62. https://doi.org/10.3390/muscles1010005

Academic Editor: Tatiana Kostrominova

Received: 5 January 2022
Accepted: 15 March 2022
Published: 17 March 2022

Publisher's Note: MDPI stays neutral with regard to jurisdictional claims in published maps and institutional affiliations.

Copyright: © 2022 by the authors. Licensee MDPI, Basel, Switzerland. This article is an open access article distributed under the terms and conditions of the Creative Commons Attribution (CC BY) license (https://creativecommons.org/licenses/by/4.0/).

1. Introduction

For any biological joint, a single degree of freedom is supported by a number of active and passive force-generating structures. Thus, a torque acting in the joint can be calculated from known external forces with ease, but the calculation of the forces of structures internal to the body is currently the focus of scientific investigation [1]. At the shoulder joint, the rotator cuff, consisting of four small muscles, is covered by three bigger parts of the deltoid muscle. Bi-articular arm and multi-articular chest and back muscles as well as a complex of ligaments act on the shoulder joint. Consequently, the unknown internal forces producing the joint torque are distributed across many force-generating structures, and in the case of external loading, the internal load scenario is further complicated.

When looking at injuries of the shoulder muscles, the rotator cuff, more specifically the supraspinatus muscle, seems to be the muscle–tendon complex (MTC) most vulnerable to failure due to high forces acting on the arm. In contrast to all other muscles of the rotator cuff, the supraspinatus tendon is caudally deflected on the head of the humerus. Thus, the muscle is vulnerable to strain produced by abduction and adduction of the arm in the frontal plane. Such movements may be initiated actively or occur in situations in which MTC loading is enforced, whether the muscle fibres are activated or not. Furthermore, the

anatomical structure of the supraspinatus tendon is inhomogeneous [2] and different areas provide different mechanical properties [3–6]. Accordingly, peak tendon forces may not be adequately represented only by the tendon cross-sectional area. This might explain peak tendon forces differing between diverse test conditions [6–8].

Moreover, the supraspinatus muscle is the smallest muscle in relation to all other muscles surrounding the glenohumeral joint. Its percentage in shoulder muscle cross-sectional area (MCSA) is only about 3.5%, and its lever arms are the shortest. It can, therefore, add not more than 5% to the maximum glenohumeral joint torque, that is, about 0.4 Nm [9]. Assuming half the arm length to be 0.25 m, the supraspinatus can, thus, lift about 160 g which is less than 10% of the arm's mass. This number may be too low by a factor of two due to MCSA data coming from elder specimen with potential muscle atrophy. Hence, other larger, more powerful muscles surrounding the glenohumeral joint must provide the main forces for the daily motions of the arm.

Muscle forces acting at the glenohumeral joint have been predicted by biomechanical models. Finite element models (FEM) calculate well the forces within different parts of the muscle fibres or the tendon [10–12]. However, highly dynamic processes cannot be simulated by the FEM method. Schouten et al. [13] calculated shoulder muscle forces optimized by an energy criterion only for the muscle fibres with a multi-body dynamic model, but the prediction of the stiffness of the muscles was to low. The Delft Shoulder and Elbow Model is well established in terms of its passive mechanics (masses and inertia) and predicts different motions in good coherence to experimental data [14,15]. Internal muscle forces were calculated by inverse dynamics and compared to signals from surface electromyography [16]. With mean r = 0.66, only low correlations were calculated, and it is questionable how well deeper muscles can be assessed by surface electromyography. Furthermore, only slow motions or poses of one subject were measured.

Aside from ethical reasons, it is delicate and costly (tendon) or practically impossible (muscle fibres) to measure the forces of structures internal to the body. Moreover, for ethical reasons, realistic accident-like situations cannot be applied to humans. Currently, therefore, more knowledge about the force distribution of different muscles acting at the shoulder joint during fast motions can only be provided by a model-based approach. In this study, computer simulations of fast motions were carried out in order to predict the forces acting within the shoulder muscles and their tendons. Predicted motions and forces acting on the elbow are compared to experimental data. Our computer model maps the anatomy of the glenohumeral joint. Additionally, the contraction and activation dynamics of four shoulder muscles are each represented by a Hill-type muscle model. Hill-type muscle models allow the simulation of a lot of muscle functions explored experimentally, such as eccentric force production [17], parallel elasticities like titin [18], muscle-fibre tendon interactions [19], complement muscle activation and exhaustion [20,21], and lateral forces [22]. The aim is to answer the following question: Can the thicker, more outer-positioned, synergistic MTC, such as the deltoid muscle, provide support or protection for the smaller, more proximal positioned supraspinatus muscle, if there are high forces acting on the arm? Moreover, situations in which the supraspinatus tendon is most vulnerable to injury can be estimated.

2. Material and Methods

2.1. Overview

To check the validity of the model predictions, different motions of the right arm were analysed experimentally. The shoulder angle and contact force of nine volunteers (5 male, 4 female) were measured (Table 1). The experimental protocol for this study was reviewed and approved by the Thuringia State Medical Association ethics committee on 3 March 2011 (protocol #37826/2011/6). All human subjects gave written informed consent prior to the participation in this study. The study was following ethical guidelines stated in the Declaration of Helsinki. The initial angular and muscle activity conditions of the shoulder model were adjusted to simulate the situations in which the subjects performed the motions. Model data were then compared to experimental data.

Table 1. Age, body height, and body weight as mean (standard deviation) for all investigated subjects.

Sex [n]	Age [Years]	Body Height [m]	Body Weight [kg]
Female (4)	28.0 (9.4)	1.70 (0.03)	67.3 (7.4)
Male (5)	29.8 (5.5)	1.87 (0.09)	82.2 (12.4)

2.2. Experiments

Different motions were analysed within the frontal plane of the body: (1) A simple side lift of a 0.5 litre water bottle at shoulder height, with elbow almost stretched; (2) pressure of the right elbow against an immovable force-measurement grip (see below)(for this, the subjects stood in a solid position and pushed the elbow, using only the forces of the shoulder joint, against the force-measurement grip); and (3) a gentle fall on the elbow. Here, the subjects stood beside the force-measurement grip without touching it. The distance, according the height and courage of the subject, between elbow and the force-measurement grip was almost 15 cm. Now, the subject had to tilt over the outer edge of the right foot to fall against the force-measurement grip with the elbow and push back to the standing position by itself. The contact point of the elbow in test situations (2) and (3) was just above *epicondylis lateralis humeri*, where there is enough soft tissue to dampen the contact with the force-measurement grip (Figure 1). The height of the force-measurement grip was adjusted to the height of the subject's elbows. All motions were repeated 25 times with breaks after every 5 single motions.

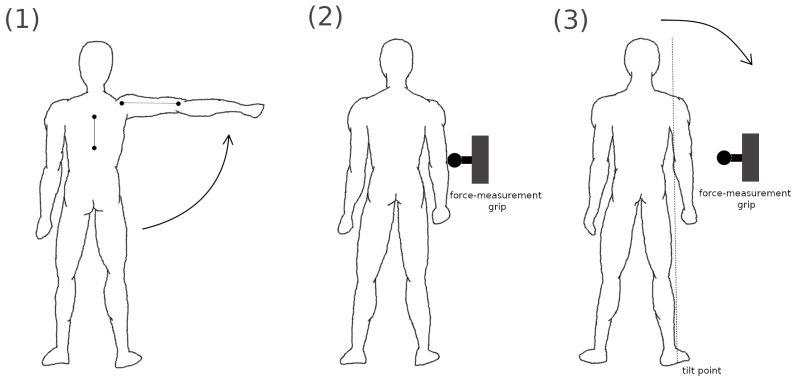

Figure 1. Sketches of the dynamic shoulder experiments of the subjects. For (1), the right arm must be elevated, black circles on the back, shoulder and the elbow show skin marker positions and corresponding vectors to calculate the shoulder angle. (2) was only the pressure of the elbow against the force-measurement grip. The gentle fall against the force-measurement grip is depicted in (3), the bottom of the dotted line marks the tilting point on the edge of the right foot.

To analyse the shoulder angle, four infra-red light emitting markers were applied on the subjects back and right arm. Marker positions were the tip of the thoracic spine on level Th8, the neck on cervical level C7, and the acromion and the backside of the elbow. The angle between vectors Th8-C7 and the acromion elbow was defined as shoulder angle. A more detailed analysis of shoulder bones such as the scapula is not reasonable due to artefacts inflicted by soft tissue's movement [1]. A further three markers were applied on the force-measurement grip for reconstructions of the positions of the subjects within the coordinate system of the force-measurement grip. Positions of the markers were recorded at 100 Hz by an infra-red light camera system (LaiTronic GmbH, Innbruck, Austria).

The contact force of the elbow was measured by a custom made force-measurement grip. The device collects data on a hand grip in three dimensions. Base force transducer devices of the force-measurement grip were three weighing platform elements (PW10AC3, Hottinger Baldwin Messtechnik GmbH, Darmstadt, Germany). Analogue signals of the weighing platform elements were amplified and sent to a signal locker (TOM, GJB Datentechnik GmbH, Langewiesen, Germany). Data collection was performed at 2048 Hz. The

value of the force vector was calculated. Synchronisation of cinematographic and force data was performed by an analogue bridge emitting a signal to both measurement devices.

2.3. Shoulder Model

The model of the shoulder is a direct dynamic model consisting of only two rigid bodies connected by a hinge joint to simulate motions of the shoulder within the frontal plane of the body. The base body is the lumped segment of head and trunk. The moving body is the right arm. Masses, inertia, and length relations were extracted from a database [23].

The main components to drive the model are Hill-type muscle models to simulate muscle–tendon complexes (MTC). Three muscles of the rotator cuff and the middle part of the deltoid muscle were implemented. MTCs of supraspinatus muscle and deltoid muscle deflect within typical conditions. Deflection calculation is point-deflection; that is, if the lever to deflect crosses the line between origin and insertion of the MTC, MTC will be deflected without friction. Deflection levers for both MTCs are connected to the solid of the upper arm. Contact force, torque, and length changes are propagated to the deflection lever in cases of deflection. The geometry of origins, insertions, and deflection points is summarised in Table 2 and Figure 2.

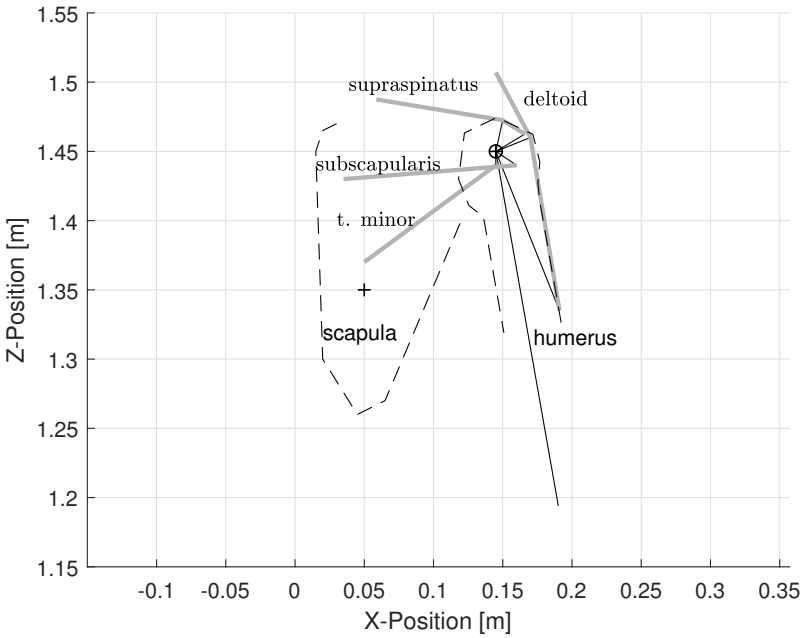

Figure 2. Geometrical arrangement of structures in the shoulder model. Offsets of the bones in relation to the ground are marked by $+$. The centre of rotation of the humerus at the scapula is indicated by $\circ$. Lever arms for deflection and insertion of the MTCs are given by solid black lines. Current lines of action of the MTCs are shown as grey thick lines.

The MTC model is based on Günther et al. [24] and used in the latest stage of development also for eccentric contractions [17]. The MTC model parameters are based on animal data [25]. Different MTC properties can be reproduced by the model (e.g., [18,25,26]). Moreover, the interaction of muscle fibres and the tendon can be simulated within different length relations [19]. Furthermore, elasticities in parallel with the muscle fibres are implemented (parallel elastic element, PEE) to simulate passive forces of the MTC if tendon and PEE are stretched [18]. Thus, the muscle model is a tool suitable for the prediction of loads within MTC (Table 3). Muscle size and length relations were extracted from the literature [27] and estimated from anatomical text books.

Table 2. Geometric arrangement of the four shoulder muscles. For each point, the relative position (depending on positions on different bodies) to the origin of the coordinate system of the corresponding body is given. All MTC origins are at the scapula, deflection and insertions is at the humerus. Accordingly, the coordinate base of the scapula is on the lower part of the bone [0.05 1.35], the coordinate base of the humerus is the centre of the head of the humerus [0.145 1.47]. The angular initial condition of the humerus is a slight abduction of 10°. All data are provided in metres for X-axis pointing to the right and Z-axis directed upwards.

MTC Relative Position	Origin [0.05 1.35]	Deflection [0.145 1.47]	Insertion [0.145 1.47]
Middle deltoid	[0.095 0.157]	[0.025 0.01]	[0.046–0.115]
Supraspinatus	[0.0087 0.1375]	[0.005 0.0225]	[0.021 0.0125]
Teres minor	[0 0.02]	-	[0–0.01]
Subscapularis	[−0.015 0.08]	-	[0.015 0.01]

Table 3. Isometric force capacity F_{max}, length relations of the MTC-models ($L_{CE,0}$, $L_{SE,0}$), and stimulation for different simulations. For each MTC, the rest length of the parallel elastic element (PEE) equals the optimal length of CE.

MTC Unit	F_{max} [N]	$L_{CE,0}$ [m]	$L_{SE,0}$ [m]	Lift (1) [-]	Press (2) [-]	Fall (3) [-]
Middle deltoid	2000	0.095	0.024	0.2	0.2	0.2
Supraspinatus	285	0.085	0.024	0.1	0.01	0.01
Teres minor	379	0.1175	0.0128	0.01	0.01	0.01
Subscapularis	379	0.105	0.027	0.05	0.05	0.05

The contact just above *epicondylis lateralis humeri* was modelled as a lever to lever contact, that is, when the position on the humerus was on the right side of the contact lever and within a plane area of 10 × 10 cm (placed vertically), a contact force between the lever on the humerus and the lever of the contact was acting. The contact force was calculated as a spring-like soft-tissue to solid contact, with $k_F = 10^7$ N/m as the non-linear spring constant, $d_k = 10^7$ N/m s^{-1} for non-linear damping, and $\nu = 3$ for each exponent [28]. The distance vector between the contact lever on the humerus and the plane of the contact area defines the contact force direction; that is, only X-components were used to calculate the contact force. The contact force value was used for comparison with data from the experiments.

For all simulations, the initial condition was an upright head-trunk segment, with the arm segment abducted by a shoulder angle of 10° (Figure 2). The simulation of lifting the water bottle (1) was performed with an additional solid (m = 0.53 kg) at the position of the model's hand. For the simulation of the pressure against the force-measurement grip (2), the position of the contact area was placed few millimetres from the corresponding lever on the humerus. For simulating the gentle fall (3), the contact area was placed 0.1 m sideways right to the lever on the humerus. To simulate the tilt of the subjects, the lumped segment of head and trunk—to which the shoulder joint is linked—was connected to a hinge joint in the position where the right foot of the subjects would stand ($X = Z = 0.0$ m; Figure 2). The centre of mass of the lumped body-segment was positioned to the right of the hinge joint (X_{COM} = 0.05 m) for the initiation of the side tilt. The starting angle of the shoulder was 10° abduction for all simulations.

The activation dynamics of the MTC are based on Hatze [29] and used in the latest version [30] after a step-wise revision process [20,31,32], where length dependence of the contractile element (CE, model for muscle fibres) is implemented. The stimulation input to the activation dynamics does not contain any regulation by higher order processing physiology (spinal cord or cortex). Stimulation generates the activation of the MTC, which is the flow of calcium ions into the muscle cell, with the fibre force increasing with calcium

concentration. Ceasing stimulation results in deactivation. The MTCs of the rotator cuff were fully stimulated right from the beginning of the simulation. The start of stimulation of the middle deltoid MTC was 250 ms after the beginning of the simulation. (Table 3). All simulations were performed with Simscape Multibody (MathWorks, Natick, MA, USA). A Dormand-Prince solver (ode45, automatic absolute tolerance, relative tolerance 10^3) with variable step size was used.

3. Results

3.1. Shoulder Angle While Lifting a Low Load

Within the variability of the nine subjects, the load was elevated within a range of 0.65 to 1.5 s. The maximum shoulder angle of the subjects was between 68° and 97°. The simple shoulder model lifts the load in the same manner the subjects were lifting the load: The model replicates the shoulder angle very well; the prediction is congruent with data of fast lifting subjects (Figure 3, left). From this, it follows that the activation dynamics used here and the resulting force characteristics of the MTCs while lifting the load reliably simulate shoulder motions.

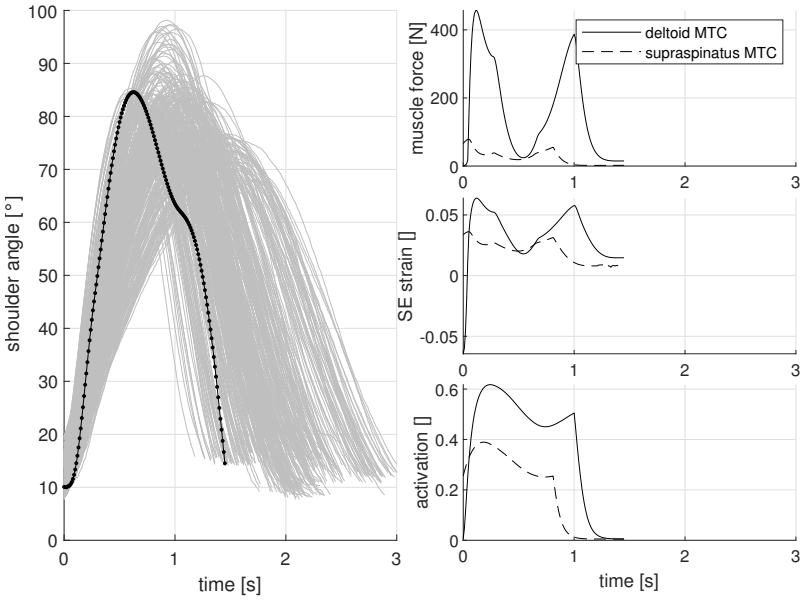

Figure 3. Left: Experimental (grey) and model data (black) of the shoulder angle while lifting a 0.53 kg load. For fast motions, the model well predicts the shoulder angle. **Right**: Forces (**top**), strain of the SE (**middle**) and activations (**bottom**) of selected MTCs. Angular change is effected by forces of the deltoid MTC mainly. Despite very low stimulation of the supraspinatus MTC (see Table 3), activation is comparable to deltoid MTC.

While the arm is lowered, the model predicts a distinct change in angular velocity when the shoulder angle is lower than 60°. Because there is no regulation of the stimulation than switch on/off in the model, a more complex stimulation pattern while lowering the arm in the subjects can be surmised. Moreover, a less fast-lifting task is not predictable by the model without tuned stimulation (not implemented in the model). Lower stimulation elevates the arm only to a lower shoulder angle. Thus, slow motions of the shoulder joint must be managed by a more complex stimulation pattern.

The model predicts almost 460 N for the deltoid muscle to lift the load. The smaller supraspinatus MTC produces only 20% the force of the deltoid MTC and would not be able to elevate the arm with the load (see F_{max} in Table 3). The strain of the serial element (SE) is almost 0.063 for the deltoid MTC and predicts a moderate load on the tendon (Figure 3, right).

3.2. Contact Force While Pushing the Force-Measurement Device

The model prediction, again, is in line with the variability of the nine subjects when pushing the elbow against an immovable grip. Fast contact force change occurs within 0.7 s and can be well predicted by the simple stimulation of MTCs. Subjects and model achieve almost 160 N (Figure 4, left).

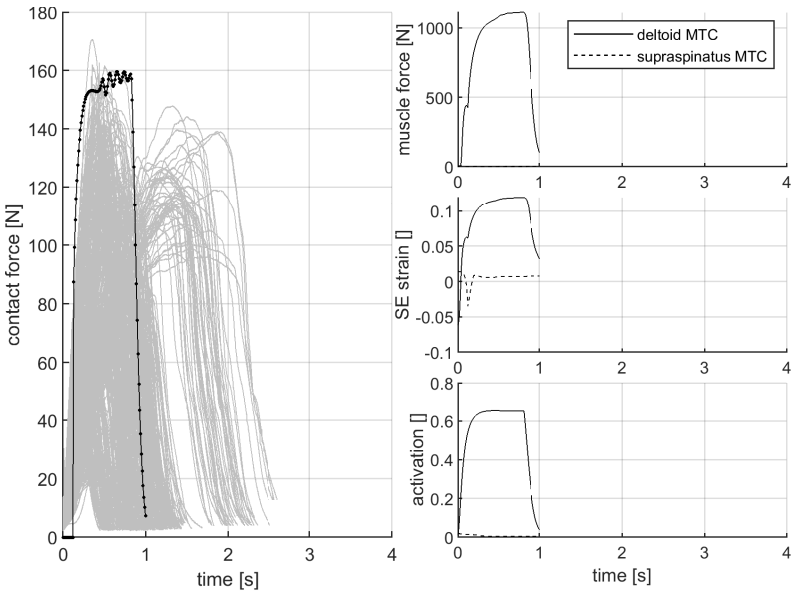

Figure 4. Left: Experimental (grey) and model data (black) of the contact force value while pushing the elbow against an immovable device. The model represents experimental data very well. **Right**: With high external force, medium activation (**bottom**), the deltoid MTC (**top**) produces medium force. From this follows moderate strain of the SE of the deltoid MTC, and the SE of the supraspinatus MTC is predicted to be slack instantly, and then to be stretched low (**middle**).

When there is slower force change at the contact position, the simple switch on/off regulation is not able to reproduce experimental data. The stimulation process for slower motions seems to be more complex than modelled here.

The inner force of the deltoid MTC achieves almost 1200 N (Figure 4, right). Performing an isometric contraction, the SE of the deltoid MTC is stretched up to 0.12, indicating a moderate to high load within the MTC.

3.3. Contact Force during the Gentle Side Fall against the Force-Measurement Device

The most vulnerable, accident-like motion for the shoulder joint was the side fall against the force measurement device. As in the quick performed experiments (depending on the courage of the subject), the model predicts a comparable contact force change within 15 ms up to 230 N. Experimental and simulation force curves (slopes) closely matched. After this, the model predicts a quick release from the contact position, whereas during some of the experiments, there was a longer contact phase. In the simulation, there is, too, a second contact, but then the lever on the model-elbow misses the contact area. Again, this difference can be caused by more careful regulation of activation by some subjects than implemented in the model. Despite this, a second peak can be found in some experiments, as predicted by the model (Figure 5, left).

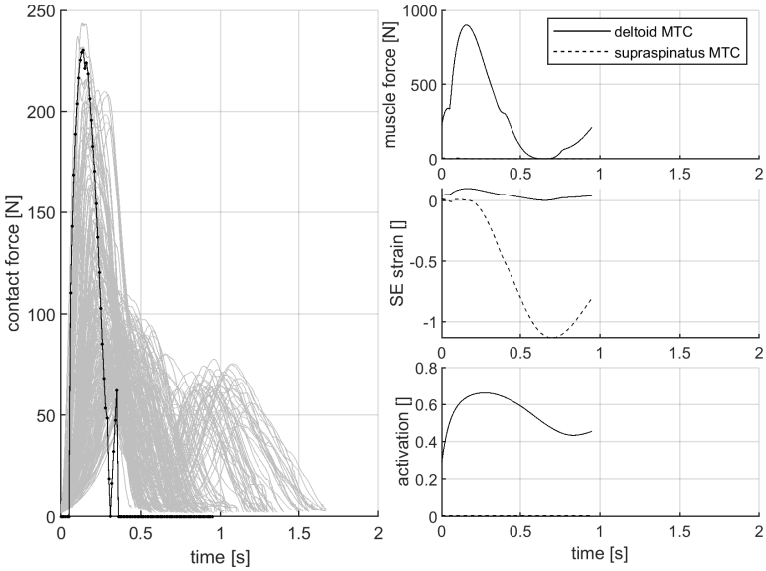

Figure 5. Left: Experimental (grey) and model data (black) of the contact force value during gentle side fall against an immovable device. Model prediction well replicates experimental data: force value and force development are in line with the experiments. **Right**: Due to the quick development of high external forces, the force of the deltoid MTC achieves almost 900 N during contact (**top**). In consequence, there is high strain of the SE of the deltoid MTC. During contact, the SE of the supraspinatus MTC is predicted to have low strain, and it is predicted, after this, to be slack (**middle**). Predicted activation is moderate for the deltoid MTC and very low for the supraspinatus MTC (**bottom**).

The external contact force is dominated by body weight and its momentum dependent on the courage of the subject. Thus, increased body weight and increased momentum results in the highest contact forces in the experiments. Despite the low activation of the deltoid MTC, it produced almost 900 N in the simulation. During contact, this inner force results in the explicit strain of the SE of the deltoid MTC. The SE of the supraspinatus MTC is predicted to be slack (Figure 5, right). Due to very short duration of such situations, MTCs are near incapable to regulate anything against the mechanical constraints acting. Moreover, forces produced due to mechanical constraints (vanishing momentum in the case of a fall on a hard surface) simply surpass the physiological limits a complex of MTCs could provide.

Taken together, the reasonable reproduction of the experimental data in all simulations provide evidence that the near-static properties of the modelled shoulder muscles realistically represent the respective physiology.

4. Discussion

4.1. Simple Hatze-Based Activation for the Simulation of Fast Motions

The simulations of shoulder movements presented here were in good congruence with experimental data, when the respective motion was performed quickly. Thus, the simple on/off regulation of the Hatze-based activation dynamics [30] is ideal for the simulation of fast motions. Fibre length dependence (FLD) of the activation dynamics used may be a reason for the good congruence reported here because the same amount of stimulation results in different activations of CE (see Figure 3, right, bottom). Thus, FLD seems to be a short duration self-regulating mechanism for quick motions during terrestrial gate or even accident-like situations. With shortening CE, activation decreases and the active force production process regulates down by itself. This seems to be advantageous, because a CE operating on the ascending limb of the force-length relation cannot produce more force actively, because it shortens and the shorter it becomes, the less force it produces.

In the simulation of the side lift (Figure 3), there is a concentric contraction, the CE of the deltoid MTC becomes shorter and, in the end, operates on the ascending limb of the force-length relation. In this situation, it mainly initiates the lowering of the arm, because the activation depends on the length of the CE. Being a time-dependent process, activation consequently decreases.

The variability of slower motions presented by the subjects could not be simulated well. To simulate slower motions, a more complex stimulation regulation is necessary. For example Biewener et al. [33], Dick et al. [34] validated Hill-type muscle models against forces deviated from sonographic fascicle force measurements by electromyography. In their study slow motions (slow CE-velocity) with high amount of stimulation showed a better congruence than fast motions. Electromyographic signals may provide a fitting activation regulation [35]. Currently, there are few well-established regulation models (e.g., Günther and Ruder [36]). The perspectives relative to neural stimulation pattern in combination with Hill-type muscle models were analysed [37], and mathematical formulations were developed [38]. For simple regulation of activation processes, a shortened CE may be an indicator for lowering the stimulation.

4.2. Mechanical Constraints as an Explanation for Tendon Damage

The highest forces within the MTC of the deltoid muscle and, accordingly, most load on the SE (tendon model), were predicted during the push and gentle fall onto the immovable device. Without high stimulation of the deltoid MTC, considerable activation and forces were also produced by fast-acting external forces (Figure 5, left).

Increased momentum, for example, during a full side fall on the elbow onto the floor, accordingly results in higher forces, which may surpass the physiological strain rate of the tendon. Such a condition may indeed be the force transmission to break the momentum with only a few structures or even only one. In the event of a non-stimulated deltoid MTC during the gentle side fall, a base stimulation of the supraspinatus MTC would be critical. The supraspinatus MTC would have to transmit the main force, if at the same time the deltoid MTCs were to be slack. The SE of the supraspinatus MTC would achieve strains of more than 0.12, an amount at which a physiological tendon would tear [39]. As a result, without extreme forces acting externally, an active deltoid MTC protects the supraspinatus MTC by carrying most of the load.

During lifting of the load, the deltoid MTC produces higher forces the more the arm is elevated, but within the most elevated configuration, the force decreases. Here, geometrical and biomechanical conditions provide an explanation: The more the arm is elevated, first the deflection turns off, and then the current lever arm becomes smaller. Only low shoulder joint torque will be generated by the deltoid MTC, despite its increasing force. Within a more elevated configuration, CE shortens to $L_{CE} = 0.05\,\mathrm{m}$ and operates on the ascending branch of the force–length relation [17]. There is no further shortening capacity of the CE; thus, the force decreases. Furthermore, the activation process decreases due to the small length of CE and results in less force production. Thus, without the rotation of the scapula, the arm can only be elevated to shoulder height.

4.3. Muscle Force Generation and Limiting Degenerative Factors

During training of older subjects, the strain rate of the patellar tendon relative to a specific force decreased and its stiffness increased [40,41]. A non-trained shoulder MTC would need more time to produce the necessary force during the motions investigated here. Moreover, the non-trained muscle fibres (CE) produce lower forces and may work on the ascending branch of the force-length relation, because the non trained SE must be stretched more than a trained SE. It is questionable whether a non-trained SE with higher strain rate and less force capacity would fail, because data pertaining to ruptures of degenerated tendon material are not available. However, in elderly people, such an awkward scenario may occur in the event of fast motions or an accident: The MTCs would need more time to

produce adequate forces; thus, the body would be positioned in a more dangerous situation. During side falls, the momentum of the body would vanish at a larger tilt angle.

Muscle fibres show loss in myosin concentration and decreased myosin–actin ratio after immobilisation, and from this, a decrease in cross sectional area results [42]. The main change is the reduced specific force of the muscle fibre [42,43]. During the tasks of this study, the shoulder muscles would produce lower forces and the time to reduce a specific amount of momentum would increase, and in turn, the body would be in a more dangerous situation (bigger tilt angle). The combination of a degenerated SE (tendon model) and detrained CE (muscle fibres) would result in a higher risk of damages to small MTCs in the event of an accident.

4.4. Limitations of This Simulation Study

The shoulder angle of the model does not fully replicate the subjects shoulder angle measured during the experiments. The model shoulder angle is only the angle of the hinge joint. In the experiments, there was no regulation of an isolated motion between the scapula and the humerus. In reality, it is impossible to move the humerus in isolation against the scapula; due to multibody motions, the scapula will be rotated. Furthermore, with a skin marker method, it is impossible to identify motions of the scapula because of soft tissue artefacts [1,44,45].

The muscle model implemented here produces its force only on the line of action, also in case of deflection. Any lateral force produced by shortening and associated bulge of the muscle fibres is not implemented. Such lateral forces may play an important role at the shoulder joint; the hat-like deltoideus muscle may produce compression on the joint and other surrounding muscles.

The representation of the shoulder model by a hinge joint does not allow any translational motion of the humerus in relation to the scapula, for example, the luxation of the humerus. Translational motions would result in a pronounced strain of soft tissue such as ligaments (not implemented) and MTCs, which would be a reason for tearing biological materials such as muscle fibres or tendon. The forces of the MTCs during the examples simulated resulted in a high strain of SE without translational excursion; moreover, during push or fall against the immovable device, the variation in shoulder joint angle was small. Thus, high external forces alone may be a cause of material damage. Again, without large muscles such as the deltoid muscle being activated, small muscles such as the supraspinatus muscle, being active or merely stretched, may experience a tear.

The implementation of ligaments was performed by Charlton and Johnson [46]. However, the scope of the Newcastle shoulder model is to provide guidance for surgery and implant design. Any active force generation within a MTC or forces due to strain in the ligaments was not in the focus of their calculations. The impossibility of predicting ligament forces on the shoulder joint seems to be caused by a lack of knowledge of forces acting within the glenohumeral ligaments. Our literature enquiry revealed only one study documenting ligament forces within static conditions [47]. Despite testing the ligaments over a broad range of shoulder angles, only small forces (almost 30 N directed anterior) were documented; the authors argue, within the physiological motions of the shoulder, that glenohumeral ligaments would not act similarly to traditional ligaments. Thus, a complete force–strain relation as known in tendons (e.g., [48]) is unknown for ligaments in the shoulder. For a solid implementation of ligaments in a shoulder model, more detailed research on its mechanical properties is necessary. To obtain an idea of how ligaments work on the shoulder, also for other joints, the connection of the force–strain relation to the joint angle is of the highest interest.

4.5. Conclusions

For fast motions, the simple shoulder model based on Hill-type muscle models, mainly, well represents motions of the shoulder joint or the load scenario quantified during the experiments. Furthermore, the inner load distribution between small and bigger shoulder

muscles can be predicted. In accident-like situations, bigger muscles, such as the deltoid muscle, have the potential to protect smaller muscles such as the supraspinatus muscle. Further research is necessary to shed light on the function of ligaments and the lateral forces of muscles at the shoulder joint.

Author Contributions: Conceptualization, F.M. and I.B.; writing—original draft preparation, F.M.; writing—review and editing, I.B.; project administration, I.B. All authors have read and agreed to the published version of the manuscript.

Funding: This research received no external funding.

Institutional Review Board Statement: The experimental protocol was reviewed and approved by the local ethics commission of Thuringia State Medical Association (Landesärztekammer Thüringen, #37826/2011/6). The exact date of the ethics approval is 3 March 2011. Landesärztekammer Thüringen).

Informed Consent Statement: All investigated subjects were volunteers and provided informed written consent after the Declaration of Helsinki.

Data Availability Statement: The data presented in this study are available in the main text, figures, tables.

Acknowledgments: Thanks to Sophie Hebel for assistance during the measurements. Thanks to Michael Günther for discussions on the manuscript. Thanks to Jeremy Thorne for language improvement.

Conflicts of Interest: The authors declare no conflict of interest.

References

1. Quental, C.; Folgado, J.; Ambrósio, J.; Monteiro, J. A multibody biomechanical model of the upper limb including the shoulder girdle. *Multibody Syst. Dyn.* **2012**, *28*, 83–108. [CrossRef]
2. Clark, J.M.; Harryman, D.T. Tendons, ligaments, and capsule of the rotator cuff. Gross and microscopic anatomy. *J. Bone Jt. Surgery. Am. Vol.* **1992**, *74*, 713–725. [CrossRef]
3. Lake, S.P.; Miller, K.S.; Elliott, D.M.; Soslowsky, L.J. Effect of fiber distribution and realignment on the nonlinear and inhomogeneous mechanical properties of human supraspinatus tendon under longitudinal tensile loading. *J. Orthop. Res.* **2009**, *27*, 1596–1602. [CrossRef] [PubMed]
4. Lake, S.P.; Miller, K.S.; Elliott, D.M.; Soslowsky, L.J. Tensile properties and fiber alignment of human supraspinatus tendon in the transverse direction demonstrate inhomogeneity, nonlinearity, and regional isotropy. *J. Biomech.* **2010**, *43*, 727–732. [CrossRef] [PubMed]
5. Lee, S.B.; Nakajima, T.; Luo, Z.P.; Zobitz, M.E.; Chang, Y.W.; An, K.N. The bursal and articular sides of the supraspinatus tendon have a different compressive stiffness. *Clin. Biomech.* **2000**, *15*, 241–247. [CrossRef]
6. Itoi, E.; Berglund, L.J.; Grabowski, J.J.; Schultz, F.M.; Growney, E.S.; Morrey, B.F.; An, K.N. Tensile properties of the supraspinatus tendon. *J. Orthop. Res.* **1995**, *13*, 578–584. [CrossRef]
7. Huang, C.Y.; Wang, V.M.; Pawluk, R.J.; Bucchieri, J.S.; Levine, W.N.; Bigliani, L.U.; Mow, V.C.; Flatow, E.L. Inhomogeneous mechanical behavior of the human supraspinatus tendon under uniaxial loading. *J. Orthop. Res.* **2005**, *23*, 924–930. [CrossRef] [PubMed]
8. Barber, F.A.; Herbert, M.A.; Boothby, M.H. Ultimate tensile failure loads of a human dermal allograft rotator cuff augmentation. *Arthroscopy* **2008**, *24*, 20–24. [CrossRef] [PubMed]
9. Bassett, R.W.; Browne, A.O.; Morrey, B.F.; An, K.N. Glenohumeral muscle force and moment mechanics in a position of shoulder instability. *J. Biomech.* **1990**, *23*, 405–415. [CrossRef]
10. Seki, N.; Itoi, E.; Shibuya, Y.; Wakabayashi, I.; Sano, H.; Sashi, R.; Minagawa, H.; Yamamoto, N.; Abe, H.; Kikuchi, K.; et al. Mechanical environment of the supraspinatus tendon: Three-dimensional finite element model analysis. *J. Orthop. Sci.* **2008**, *13*, 348–353. [CrossRef]
11. Sano, H.; Wakabayashi, I.; Itoi, E. Stress distribution in the supraspinatus tendon with partial-thickness tears: An analysis using two-dimensional finite element model. *J. Shoulder Elb. Surg.* **2006**, *15*, 100–105. [CrossRef] [PubMed]
12. Wakabayashi, I.; Itoi, E.; Sano, H.; Shibuya, Y.; Sashi, R.; Minagawa, H.; Kobayashi, M. Mechanical environment of the supraspinatus tendon: A two-dimensional finite element model analysis. *J. Shoulder Elb. Surg.* **2003**, *12*, 612–617. [CrossRef]
13. Schouten, A.C.; de Vlugt, E.; van der Helm, F.C.; Brouwn, G.G. Optimal posture control of a musculo-skeletal arm model. *Biol. Cybern.* **2001**, *84*, 143–152. [CrossRef] [PubMed]
14. Nikooyan, A.A.; Veeger, H.E.J.; Westerhoff, P.; Graichen, F.; Bergmann, G.; van der Helm, F.C.T. Validation of the Delft Shoulder and Elbow Model using in-vivo glenohumeral joint contact forces. *J. Biomech.* **2010**, *43*, 3007–3014. [CrossRef] [PubMed]
15. Bolsterlee, B.; Veeger, H.E.J.; van der Helm, F.C.T. Modelling clavicular and scapular kinematics: From measurement to simulation. *Med. Biol. Eng. Comput.* **2014**, *52*, 283–291. [CrossRef] [PubMed]

16. Nikooyan, A.A.; Veeger, H.E.J.; Chadwick, E.K.J.; Praagman, M.; van der Helm, F.C.T. Development of a comprehensive musculoskeletal model of the shoulder and elbow. *Med. Biol. Eng. Comput.* **2011**, *49*, 1425–1435. [CrossRef] [PubMed]
17. Haeufle, D.F.B.; Günther, M.; Bayer, A.; Schmitt, S. Hill-type muscle model with serial damping and eccentric force-velocity relation. *J. Biomech.* **2014**, *47*, 1531–1536. [CrossRef]
18. Rode, C.; Siebert, T.; Herzog, W.; Blickhan, R. The effects of parallel and series elastic components on the active cat soleus force-length relationship. *J. Mech. Med. Biol.* **2009**, *9*, 105–122. [CrossRef]
19. Mörl, F.; Siebert, T.; Häufle, D. Contraction dynamics and function of the muscle-tendon complex depend on the muscle fibre-tendon length ratio: A simulation study. *Biomech. Model Mechanobiol.* **2015**, *15*, 245–258. [CrossRef]
20. Rockenfeller, R.; Günther, M. Hill equation and Hatze's muscle activation dynamics complement each other: Enhanced pharmacological and physiological interpretability of modelled activity-pCa curves. *J. Theor. Biol.* **2017**, *431*, 11–24. [CrossRef]
21. Rockenfeller, R.; Günther, M.; Stutzig, N.; Haeufle, D.F.B.; Siebert, T.; Schmitt, S.; Leichsenring, K.; Böl, M.; Götz, T. Exhaustion of skeletal muscle fibers within seconds: Incorporating phosphate kinetics into a Hill-type model. *Front. Physiol.* **2020**, *11*, 306. [CrossRef] [PubMed]
22. Siebert, T.; Stutzig, N.; Rode, C. A hill-type muscle model expansion accounting for effects of varying transverse muscle load. *J. Biomech.* **2018**, *66*, 57–62. [CrossRef] [PubMed]
23. NASA. *Man-Systems Integration Standards, Anthropometry and Biomechanics*; Technical Report; National Aeronautics and Space Administration: Washington, DC, USA, 2000.
24. Günther, M.; Schmitt, S.; Wank, V. High-frequency oscillations as a consequence of neglected serial damping in Hill-type muscle models. *Biol. Cybern.* **2007**, *97*, 63–79. [CrossRef] [PubMed]
25. Siebert, T.; Rode, C.; Herzog, W.; Till, O.; Blickhan, R. Nonlinearities make a difference: Comparison of two common Hill-type models with real muscle. *Biol. Cybern.* **2008**, *98*, 133–143. [CrossRef] [PubMed]
26. Mörl, F.; Siebert, T.; Schmitt, S.; Blickhan, R.; Günther, M. Electro-mechanical delay in Hill-type muscle models. *J. Mech. Med. Biol.* **2012**, *12*, 1250085. [CrossRef]
27. Van der Helm, F.C.; Veeger, H.E.; Pronk, G.M.; Van der Woude, L.H.; Rozendal, R.H. Geometry parameters for musculoskeletal modelling of the shoulder system. *J. Biomech.* **1992**, *25*, 129–144. [CrossRef]
28. Kleinau, J. Modellierung des Mechanischen Bewegungsablaufs in Einem Arm bei Anlegen von Vibrationen Sowie Experimentelle Anpassung der Modellparameter. Master's Thesis, Eberhard-Karls-Universität Tübingen, Tübingen, Germany, 1993.
29. Hatze, H. *Myocybernetic Control Models of Skeletal Muscle—Characteristics and Applications*; University of South Africa Press: Pretoria, South Africa, 1981.
30. Rockenfeller, R.; Günther, M. Inter-filament spacing mediates calcium binding to troponin: A simple geometric-mechanistic model explains the shift of force-length maxima with muscle activation. *J. Theor. Biol.* **2018**, *454*, 240–252. [CrossRef] [PubMed]
31. Rockenfeller, R.; Günther, M. Extracting low-velocity concentric and eccentric dynamic muscle properties from isometric contraction experiments. *Math. Biosci.* **2016**, *278*, 77–93. [CrossRef] [PubMed]
32. Rockenfeller, R.; Günther, M.; Schmitt, S.; Götz, T. Comparative sensitivity analysis of muscle activation dynamics. *Comput. Math. Methods Med.* **2015**, *4*, 1–16. [CrossRef]
33. Biewener, A.A.; Wakeling, J.M.; Lee, S.S.; Arnold, A.S. Validation of Hill-type muscle models in relation to neuromuscular recruitment and force-velocity properties: Predicting patterns of in vivo muscle force. *Integr. Comp. Biol.* **2014**, *54*, 1072–1083. [CrossRef]
34. Dick, T.J.M.; Biewener, A.A.; Wakeling, J.M. Comparison of human gastrocnemius forces predicted by Hill-type muscle models and estimated from ultrasound images. *J. Exp. Biol.* **2017**. [CrossRef] [PubMed]
35. Wakeling, J.M.; Uehli, K.; Rozitis, A.I. Muscle fibre recruitment can respond to the mechanics of the muscle contraction. *J. R. Soc. Interface* **2006**, *3*, 533–544. [CrossRef] [PubMed]
36. Günther, M.; Ruder, H. Synthesis of two-dimensional human walking: A test of the lambda-model. *Biol. Cybern.* **2003**, *89*, 89–106. [CrossRef] [PubMed]
37. Brändle, S.; Schmitt, S.; Müller, M.A. A systems-theoretic analysis of low-level human motor control: Application to a single-joint arm model. *J. Math. Biol.* **2020**, *80*, 1139–1158. [CrossRef]
38. Walter, J.; Günther, M.; Haeufle, D.F.B.; Schmitt, S. A geometry- and muscle-based control architecture for synthesising biological movement. *Biol. Cybern.* **2021**, *115*, 7–37. [CrossRef] [PubMed]
39. Ker, R.F.; Wang, X.T.; Pike, A.V. Fatigue quality of mammalian tendons. *J. Exp. Biol.* **2000**, *203*, 1317–1327. [CrossRef] [PubMed]
40. Reeves, N.D.; Maganaris, C.N.; Narici, M.V. Effect of strength training on human patella tendon mechanical properties of older individuals. *J. Physiol.* **2003**, *548*, 971–981. [CrossRef] [PubMed]
41. Reeves, N.D.; Narici, M.V.; Maganaris, C.N. Strength training alters the viscoelastic properties of tendons in elderly humans. *Muscle Nerve* **2003**, *28*, 74–81. [CrossRef] [PubMed]
42. Brocca, L.; Longa, E.; Cannavino, J.; Seynnes, O.; de Vito, G.; McPhee, J.; Narici, M.; Pellegrino, M.A.; Bottinelli, R. Human skeletal muscle fibre contractile properties and proteomic profile: Adaptations to 3 weeks of unilateral lower limb suspension and active recovery. *J. Physiol.* **2015**, *593*, 5361–5385. [CrossRef] [PubMed]
43. Hvid, L.G.; Ørtenblad, N.; Aagaard, P.; Kjaer, M.; Suetta, C. Effects of ageing on single muscle fibre contractile function following short-term immobilisation. *J. Physiol.* **2011**, *589*, 4745–4757. [CrossRef] [PubMed]

44. Matsui, K.; Shimada, K.; Andrew, P.D. Deviation of skin marker from bone target during movement of the scapula. *J. Orthop. Sci.* **2006**, *11*, 180–184. [CrossRef] [PubMed]
45. Günther, M.; Sholukha, V.; Keßler, D.; Wank, V.; Blickhan, R. Dealing with skin motion and wobbling masses in inverse dynamics. *J. Mech. Med. Biol.* **2003**, *3*, 309–335. [CrossRef]
46. Charlton, I.W.; Johnson, G. A model for the prediction of the forces at the glenohumeral joint. *Proc. Inst. Mech. Eng. Part J. Eng. Med.* **2006**, *220*, 801–812. [CrossRef] [PubMed]
47. Debski, R.E.; Wong, E.K.; Woo, S.L.Y.; Sakane, M.; Fu, F.H.; Warner, J.J. In situ force distribution in the glenohumeral joint capsule during anterior-posterior loading. *J. Orthop. Res.* **1999**, *17*, 769–776. [CrossRef] [PubMed]
48. Ker, R.F. The design of soft collagenous load-bearing tissues. *J. Exp. Biol.* **1999**, *202*, 3315–3324. [CrossRef] [PubMed]